THE ROLE OF INERTIA AND DISSIPATION IN THE DYNAMICS OF THE DIRECTOR FOR A NEMATIC LIQUID CRYSTAL COUPLED WITH AN ELECTRIC FIELD

P. AURSAND AND J. RIDDER

Abstract. We consider the dynamics of the director in a nematic liquid crystal when under the influence of an applied electric field. Using an energy variational approach we derive a dynamic model for the director including both dissipative and inertial forces.

A numerical scheme for the model is proposed by extending a scheme for a related variational wave equation. Numerical experiments are performed studying the realignment of the director field when applying a voltage difference over the liquid crystal cell. In particular, we study how the relative strength of dissipative versus inertial forces influence the time scales of the transition between the initial configuration and the electrostatic equilibrium state.

1. Introduction

Liquid crystal refers to a state of matter that exhibits free flow similarly to a liquid, but with certain crystalline properties commonly associated with solids. In the nematic liquid crystal state, the long axis of the constituent molecules tend to align. This results in long-range orientational order with no long-range correlation of the centre-of-mass. In the classical continuum theory, the configuration of a nematic liquid crystal is described by a velocity field and a director field.

The behaviour of a finite sample of a liquid crystal under the influence of an electric field is of particular importance. When applying an electric field there is a competition between the boundary energy and the elastic and electrostatic forces. In the *Fréedericksz* transition, the liquid crystal cell will realign when the applied field (electric or magnetic) is above a certain critical threshold. These kinds of switching-phenomena under applied fields are of great importance because of the application to Liquid Crystal Displays (LCDs).

In this paper we will focus on the director field and use numerical experiments to simulate its dynamics under the influence of an electric field. In particular, we aim to quantify the influence of the inertia term in comparison with the dissipation term on the dynamics of the director when the electric field is switched on. The present model is derived from the Oseen–Frank elastic energy, the electric energy, and a dissipation function by the least action principle and the principle of maximum dissipation. The resulting equation can be seen as a special case of the classical Ericksen-Leslie dynamic equations. More precisely, for a planar director field ψ and an electric potential U depending only on one space variable x and time, we will derive the equation

$$\sigma\psi_{tt} + \kappa\psi_t - c(\psi)(c(\psi)\psi_x)_x - \frac{1}{2}d'(\psi)U_x^2 = 0\,, \tag{1}$$

where

$$c(\psi) = \sqrt{\alpha \cos^2(\psi) + \beta \sin^2(\psi)}\,, \quad d(\psi) = \varepsilon_0(\varepsilon_\perp + \varepsilon_a \cos^2(\psi))\,,$$

and σ is an inertial constant, κ is a dissipation coefficient, α and β are the bend and splay elastic constants, ε_0 is the vacuum permittivity, and $\varepsilon_\perp$ and ε_a are dielectric constants.

The current model is closely related to the variational wave equation

$$\psi_{tt} - c(\psi)(c(\psi)\psi_x)_x = 0\,. \tag{2}$$

This equation was first introduced by Saxton [24], and has since been subject to a considerable amount of research, see, e.g., [12, 8, 10, 11]. In the current context, (2) can be seen as a special case of (1) when there is neither an electric field nor dissipation. Also, Chen and Zheng [2] investigated the equations without electric field that include both inertia and dissipation.

Disregarding inertial terms is almost ubiquitous in the modeling of nematic liquid crystals, and herein lies the main interest of the present paper. The behavior of nematics under an electric field has been studied extensively during the last decades [4, 5, 6, 3, 25, 23]. However, to the authors' knowledge, analytical and numerical investigations have mostly been conducted for the static equations to find equilibrium solutions or for the parabolic equations where the inertia of the director is neglected. As discussed by Gang et al. [7] and van Doorn [26], in many cases there are good physical reasons why these terms are neglected. However, it was early noted by Leslie [19] that the rotational kinetic energy might play a role when the director is subjected to large accelerations. More recently, its relevance has been argued specifically in the modeling of liquid crystals under mechanical vibrations [27], acoustics [20], and, more generally, for liquid crystals with large moment of inertia that are subject to high-frequency excitation [1]. In general, inertial effects become more significant for problems of certain geometrical scalings, e.g., for very small time scales. The main purpose of this paper is to study a model which includes both inertial and dissipative terms. Moreover, we will not restrict ourselves to the one-constant approximation, which is commonly used in the literature as a simplification. Through numerical experiments using a non-dimensional form of the equations, we wish to study the transition from the viscosity-dominated regime to the inertia-dominated regime.

The basic equation derived in this work can also be derived from the general theory of anisotropic fluids, see, e.g., the fundamental work of McMillan [21]. The novel contribution of this paper lies first and foremost in the systematic numerical study of the qualitative and quantitative influence of inertia in these models for a standard test case. To do this we arguably push some physical parameters beyond the scope of present day liquid crystal devices (e.g. sub-nanosecond time scales), as was also done in the related work by Lenzi and Barbero [18].

To keep the focus on the influence of the inertia and dissipative term on the dynamics of the director field, we have restricted ourselves to a simplified setting. In the general case, the coupling between velocity and director field can lead to complicated effects, but for simplicity we will in this work assume that the velocity field is zero. In the case of the splay Fréedericksz transition this means that we neglect the so called backflow and kickback effects, which can be physically reasonable under some circumstances [25]. Furthermore, we restrict our study to a director and an electric field that vary only in one space dimension, x, and assume

that the director lies in the $x-y$ plane, while the electric field only has a component in x direction. This last assumption also implies that Maxwell's equations, which govern the electric field, reduce to the stationary equations. In other words, the electric field is assumed to be in constant electrostatic equilibrium with the changing director field.

The outline of the paper is as follows. In Section 2 we will present the derivation of our model using the least action principle and the maximum dissipation principle with the Oseen–Frank energy, the electric energy and Maxwell's equations, and a dissipation function as starting point. We will also derive a non-dimensional form of the equations, which we will be more convenient in the numerical experiments. Section 3 contains a suggested numerical method which can be used for the model. The scheme is adapted from a numerical method used for the nonlinear variational wave equation (2). In Section 4 we present results of numerical experiments of the Fréedericksz transition from a homogeneous initial state when applying an electric field. The observed time scales of the transition are compared to a linear analysis. Furthermore, in Section 5, we perform similar numerical experiments on a transition in a pi-cell when applying an electric field.

2. The model

2.1. **The general approach.** We will derive the model for the director field of a nematic liquid crystal using the least action principle for the conservative part of the equation and the maximum dissipation principle that allows us to include the effect of dissipation. To do this, we need to determine the free energy of the liquid crystal, which is the sum of the kinetic energy, the Oseen-Frank elastic energy, and the electric energy.

In the following, $\mathbf{n}(x,t)$ denotes the director field of the liquid crystals. Note that at any point in time and space, $\mathbf{n}$ has unit length, i.e., $\mathbf{n}\cdot\mathbf{n}=1$. For simplicity, we will assume that the liquid crystal does not flow, i.e., the fluid velocity is zero. The kinetic energy for the director is then given by

$$K = \frac{1}{2}\sigma|\mathbf{n}_t|^2\,, \tag{3}$$

where σ denotes an inertial constant. A typical value for σ is $\sim 10^{-13}\,\mathrm{kg\,m^{-1}}$ (for the nematic MBBA [7]). The Oseen-Frank elastic energy, which describes the tendency of the directors to align parallel, is

$$W_{OF} = \frac{1}{2}\alpha|\mathbf{n}\times(\nabla\times\mathbf{n})|^2 + \frac{1}{2}\beta(\nabla\cdot\mathbf{n})^2 + \frac{1}{2}\gamma(\mathbf{n}\cdot(\nabla\times\mathbf{n}))^2\,, \tag{4}$$

where α, β, and γ are the Frank elastic constants for bend, splay, and twist, typical values being $8.2\times10^{-12}\,\mathrm{N}$, $6.2\times10^{-12}\,\mathrm{N}$, and $3.9\times10^{-12}\,\mathrm{N}$, respectively (for 5CB [25]). The contribution to the total energy density from the electric field is given by

$$W_{el} = -\frac{1}{2}\mathbf{D}\cdot\mathbf{E}\,, \tag{5}$$

where $\mathbf{E}$ is the electric field and $\mathbf{D}$ is the electric displacement. For a uniaxial nematic, if we consider only dielectric contributions to the polarization, $\mathbf{D}$ is related to $\mathbf{E}$ through

$$\mathbf{D} = \varepsilon_0(\varepsilon_\perp\mathbf{E} + \varepsilon_a(\mathbf{n}\cdot\mathbf{E})\mathbf{n})\,, \tag{6}$$

where $\varepsilon_0 = 8.854 \times 10^{-12}\,\mathrm{F\,m^{-1}}$ is the permittivity in free space, $\varepsilon_\perp$ is the relative permittivity perpendicular to the director ($\varepsilon_\perp = 7$ for 5CB [25]) and ε_a is the dielectric anisotropy ($\varepsilon_a = 11.5$ for 5CB [25]). The electric displacement is also subject to Gauss' law, which reads (in the absence of free charges)

$$\nabla \cdot \mathbf{D} = 0\,. \tag{7}$$

Altogether, the total free energy is

$$\mathcal{E} = \int \left(K(\mathbf{n}_t) + W_{OF}(\mathbf{n}, \nabla\mathbf{n}) + W_{el}(\mathbf{n})\right)\,\mathrm{d}x\,,$$

with the corresponding Lagrangian $\mathcal{L} = K(\mathbf{n}_t) - W_{OF}(\mathbf{n}, \nabla\mathbf{n}) - W_{el}(\mathbf{n})$. The conservative system would then be described by the Euler-Lagrange equation

$$\frac{\mathrm{d}}{\mathrm{d}t}\left(\frac{\partial\mathcal{L}}{\partial\mathbf{n}_t}\right) + \frac{\mathrm{d}}{\mathrm{d}x}\left(\frac{\partial\mathcal{L}}{\partial\mathbf{n}_x}\right) + \frac{\mathrm{d}}{\mathrm{d}y}\left(\frac{\partial\mathcal{L}}{\partial\mathbf{n}_y}\right) + \frac{\mathrm{d}}{\mathrm{d}z}\left(\frac{\partial\mathcal{L}}{\partial\mathbf{n}_z}\right) - \frac{\partial\mathcal{L}}{\partial\mathbf{n}} = 0\,,$$

which is derived from the least action principle for the action functional $\mathcal{A} = \int L\,\mathrm{d}x$. For dissipative systems we can write the energy law

$$\frac{\mathrm{d}}{\mathrm{d}t}\left(\int \left(K(\mathbf{n}_t) + W_{OF}(\mathbf{n}, \nabla\mathbf{n}) + W_{el}(\mathbf{n})\right)\,\mathrm{d}x\right) = -\int \mathcal{D}(\mathbf{n}_t)\,\mathrm{d}x \tag{8}$$

for some non-negative dissipation function $\mathcal{D}(\mathbf{n}_t)$. To obtain the evolution equation corresponding to (8), it is common practice [16, 13, 22, 28] to apply Onsager's maximum dissipation principle to incorporate it in the Euler-Lagrange equation by

$$\frac{\mathrm{d}}{\mathrm{d}t}\left(\frac{\partial\mathcal{L}}{\partial\mathbf{n}_t}\right) + \frac{\mathrm{d}}{\mathrm{d}x}\left(\frac{\partial\mathcal{L}}{\partial\mathbf{n}_x}\right) + \frac{\mathrm{d}}{\mathrm{d}y}\left(\frac{\partial\mathcal{L}}{\partial\mathbf{n}_y}\right) + \frac{\mathrm{d}}{\mathrm{d}z}\left(\frac{\partial\mathcal{L}}{\partial\mathbf{n}_z}\right) - \frac{\partial\mathcal{L}}{\partial\mathbf{n}} = -\frac{\partial\mathcal{D}}{\partial\mathbf{n}_t}\,.$$

In the present case the dissipation function, as given, e.g., in [25], is

$$\mathcal{D} = \frac{1}{2}\kappa|\mathbf{n}_t|^2\,, \tag{9}$$

where $\kappa > 0$ is a viscosity coefficient (for MBBA, $\kappa = 0.0777\,\mathrm{Pa\,s}$, [25]).

2.2. **The one-dimensional case.** For the experiments in this paper, we restrict ourselves to the one-dimensional case, i.e., we assume that both the director field and the electric field depend only on the x-coordinate and time. Furthermore, we will assume that the electric field can be written as the gradient of a scalar potential and hence only has a component in the x-direction. This simplifies the equations considerably, but still allows us to model physically interesting phenomena, like the Fréedericksz transition. More precisely, we consider a liquid crystal cell that only differs in x dimension on an interval $[0, L]$ and assume that the director field is strongly anchored at the boundary, i.e., we have Dirichlet boundary conditions $\mathbf{n}(0,t) = \mathbf{n}_0$ and $\mathbf{n}(L,t) = \mathbf{n}_L$. We assume further that the director lies in the xy plane and thus can be described by an angle $\psi(x,t)$ through

$$\mathbf{n}(x,t) = (\cos(\psi(x,t)), \sin(\psi(x,t)), 0)\,.$$

Expressed in terms of ψ, the kinetic energy (3) and the Oseen-Frank energy (4) then become

$$K = \frac{1}{2}\sigma\psi_t^2\,, \quad W_{OF} = \frac{1}{2}c^2(\psi)\psi_x^2\,,$$

where

$$c(\psi) = \sqrt{\alpha\cos^2(\psi) + \beta\sin^2(\psi)}\,.$$

We write $\mathbf{E}$ as the gradient of an electric potential U, i.e.,

$$\mathbf{E}(x,t) = (E(x,t),0,0) = -\nabla U(x,t) = (U(x,t)_x,0,0)\,.$$

with boundary conditions $U(0,t)=0$ and $U(L,t)=V_0>0$, corresponding to the applied voltage. The electric displacement (6) is then given by

$$\mathbf{D}(x,t) = (-d(\psi)U_x, \frac{1}{2}d'(\psi)U_x, 0)\,,$$

where $d(\psi)=\varepsilon_0(\varepsilon_\perp+\varepsilon_a\cos^2(\psi))$. The electric energy (5), written in terms of ψ, becomes

$$W_{el} = -\frac{1}{2}d(\psi)U_x^2\,.$$

In addition, due to Gauss' law (7), the electric potential must satisfy

$$(d(\psi)U_x)_x = 0\,, \tag{10}$$

which implies

$$U(x) = \int_0^x \frac{C}{d(\psi(\xi))}\,\mathrm{d}\xi + U(0)\,, \quad \text{where} \quad C = \left(\int_0^L \frac{1}{d(\psi(\xi))}\,\mathrm{d}\xi\right)^{-1} U(L)\,. \tag{11}$$

Finally, insert the Lagrangian,

$$\mathcal{L}(\psi_t,\psi_x,\psi) = K - W_{OF} - W_{el} = \frac{1}{2}\left(\sigma\psi_t^2 - c^2(\psi)\psi_x^2 + d(\psi)U_x^2\right)\,,$$

and the dissipation function (9),

$$\mathcal{D}(\psi_t) = \frac{1}{2}\kappa\psi_t^2\,,$$

into the modified Euler-Lagrange equation for the dissipative system,

$$\frac{\mathrm{d}}{\mathrm{d}t}\left(\frac{\partial\mathcal{L}}{\partial\psi_t}\right) + \frac{\mathrm{d}}{\mathrm{d}x}\left(\frac{\partial\mathcal{L}}{\partial\psi_x}\right) - \frac{\partial\mathcal{L}}{\partial\psi} = -\frac{\partial\mathcal{D}}{\partial\psi_t}\,,$$

to arrive at the equation for the director field,

$$\sigma\psi_{tt} + \kappa\psi_t - c(\psi)(c(\psi)\psi_x)_x - \frac{1}{2}d'(\psi)U_x^2 = 0\,. \tag{12}$$

Note that in the derivation we followed common practice and neglected the dependency of U on ψ.

2.3. **The nondimensional form.** To quantify the impact of the inertial constant in comparison with the dissipation constant, we derive a nondimensional version of the equation (12). As scaling parameters, we use the interval length L, the electric potential at the boundary, V_0, and some fixed time scale τ, which results in the dimensionless length $X = x/L$, electric potential $u = U/V_0$, and time $T = t/\tau$. Furthermore, define

$$\tilde{c}(\psi) = \sqrt{\cos^2(\psi) + \frac{\beta}{\alpha}\sin^2(\psi)}\,, \quad \tilde{d}(\psi) = 1 + \frac{\varepsilon_a}{\varepsilon_\perp}\cos^2(\psi)$$

and the parameters

$$\tilde{\kappa} = \frac{\kappa\tau}{\sigma}, \quad \tilde{\lambda} = \frac{\tau}{L}\left(\frac{\alpha}{\sigma}\right)^{1/2}, \quad \tilde{\varepsilon} = \frac{1}{2}\frac{\tau^2}{L^2}\frac{\varepsilon_0\varepsilon_\perp}{\sigma}V_0^2\,.$$

Then, equation (12) is equivalent to

$$\psi_{TT} + \tilde{\kappa}\psi_T - \tilde{\lambda}^2\tilde{c}(\psi)(\tilde{c}(\psi)\psi_X)_X - \tilde{\varepsilon}\tilde{d}'(\psi)\,(u_X)^2 = 0\,. \tag{13}$$

Similarly, (10) and (11) become

$$(\tilde{d}(\psi)u_X)_X = 0\,, \quad \text{i.e.,} \quad u(X) = \Big(\int_{[0,1]} \frac{1}{\tilde{d}(\psi(\xi))}\,\mathrm{d}\xi\Big)^{-1} \int_0^X \frac{1}{\tilde{d}(\psi(\xi))}\,\mathrm{d}\xi\,. \tag{14}$$

If $\sigma \sim 10^{-13}\,\mathrm{kg\,m^{-1}}$ and $\kappa \sim 10^{-1}\,\mathrm{Pa\,s}$, as it is the case for example for MBBA or 5CB, then $\tilde{\kappa} \sim 1$ for $\tau \sim 10^{-12}\,\mathrm{s}$, i.e., for very small time scales. For materials with larger moment of inertia, the time scale corresponding to $\tilde{\kappa} \sim 1$ increases.

2.4. **The inertialess model.** In many physical situations it is argued that the inertia is negligible, i.e., $\sigma \approx 0$ and $\tilde{\kappa}, \tilde{\lambda}, \tilde{\varepsilon} \gg 1$. Then the term ψ_{TT} in the above equations vanishes and (13) reduces to

$$\tilde{\kappa}\psi_T - \tilde{\lambda}^2\tilde{c}(\psi)(\tilde{c}(\psi)\psi_X)_X - \tilde{\varepsilon}\tilde{d}'(\psi)\,(u_X)^2 = 0\,. \tag{15}$$

which is the model that is widely applied in the literature and that we will use to compare our numerical results.

3. Numerical scheme

We proceed to derive a numerical scheme for solving the non-dimensional equations (13)–(14). Introducing the auxiliary variables $v = \psi_T$ and $w = \tilde{\lambda}\tilde{c}(\psi)\psi_X$, we can rewrite (13) as a system of first-order equations,

$$\begin{aligned} v_T + \tilde{\kappa}v - \tilde{\lambda}(\tilde{c}(\psi)w)_X &= -\tilde{\lambda}\tilde{c}(\psi)_X w - \tilde{\varepsilon}\tilde{d}'(\psi)(u_X)^2\,, \\ w_T - \tilde{\lambda}(\tilde{c}(\psi)v)_X &= 0\,, \\ \psi_T &= v\,, \end{aligned} \tag{16}$$

which we want to solve for $X \in [0,1]$, $T > 0$, and some given initial data $\psi_0(X)$. As a basic first-order scheme, we adapt a semi-discrete energy preserving method presented by Koley et al. [15]. This scheme was developed for the variational wave equation

$$\psi_{tt} - c(\psi)\,(c(\psi)\psi_x)_x = 0, \tag{17}$$

but it extends straightforwardly to the present case with an electric field and dissipation term.

Let $\Delta X = 1/N$ for some positive integer N and denote any grid function $f_j(T) = f(j\Delta X, T)$. Furthermore, we introduce the shorthands

$$\bar{a}_{j+1/2} = \frac{a_{j+1} + a_j}{2}$$

and the interface jump

$$[\![a]\!]_{j+1/2} = a_{j+1} - a_j.$$

Now let $u_{X,j}$ be the discrete electric field given by

$$u_{X,j} = \left(\sum_{i=0}^{N} \frac{1}{\bar{\tilde{d}}(\psi_i)}\right)^{-1} \sum_{i=0}^{j} \frac{1}{\bar{\tilde{d}}(\psi_i)}\,. \tag{18}$$

The evolution of the semi-discrete approximations v_j, w_j and ψ_j is then given by the scheme

$$\begin{aligned}(v_j)_T + \tilde{\kappa} v_j - \frac{\tilde{\lambda}}{\Delta X}\left(\overline{\tilde{c}}_{j+1/2}\overline{w}_{j+1/2} - \overline{\tilde{c}}_{j-1/2}\overline{w}_{j-1/2}\right) \\ = -\frac{\tilde{\lambda}}{2\,\Delta X}\left(\llbracket\tilde{c}\rrbracket_{j+1/2}\overline{w}_{j+1/2} + \llbracket\tilde{c}\rrbracket_{j-1/2}\overline{w}_{j-1/2}\right) + \tilde{\varepsilon}\tilde{d}'(\psi_j)\left(u_{X,j}\right)^2,\end{aligned} \tag{19}$$

$$(w_j)_T - \frac{1}{\Delta X}\left(\overline{\tilde{c}v}_{j+1/2} - \overline{\tilde{c}v}_{j-1/2}\right) = 0 \tag{20}$$

and

$$(\psi_j)_T = v_j. \tag{21}$$

For the temporal integration, we let

$$\Delta T = \frac{\Delta X}{\tilde{\lambda}\left(1 + \frac{\beta}{\alpha}\right)} \tag{22}$$

and denote $T^n = n\Delta T$ and a fully discrete grid function as $f_j^n = f_j(n\Delta T)$. The semi-discrete form $(u_j)_T = g(u)$ is integrated using the third-order SSP Runge–Kutta scheme [9]

$$\begin{aligned}u^* &= u_j^n + \Delta T\, g(u^n)\\ u^{**} &= \frac{3}{4}u_j^n + \frac{1}{4}u^* + \frac{1}{4}\Delta T\, g\left(u^*\right)\\ u_j^{n+1} &= \frac{1}{3}u_j^n + \frac{2}{3}u^{**} + \frac{2}{3}\Delta T\, g\left(u^{**}\right).\end{aligned}$$

4. Fréedericksz transition from homogeneous initial state

Consider a liquid crystal cell initially in a near homogeneous state. When a sufficiently large electric field is applied, the Fréedericksz transition changes the director configuration corresponding to a new electrostatic equilibrium. We venture to use the current model to study the dynamics of this transition in the case of significant inertial forces. To be precise, we consider the initial-boundary problem

$$\begin{cases}\psi_{TT} + \tilde{\kappa}\psi_T - \tilde{\lambda}^2\tilde{c}(\psi)\left(\tilde{c}(\psi)\psi_X\right)_X - \tilde{\varepsilon}\tilde{d}'(\psi)u_X^2 = 0, & (X,T) \in [0,1]\times[0,\infty)\\ u_X = \frac{1}{\tilde{d}(\psi)}\left(\int_{[0,1]}\frac{1}{\tilde{d}(\psi)}\mathrm{d}\xi\right)^{-1} & \\ \psi(X,0) = \frac{\pi}{2} + \delta\sin(\pi X) & X \in [0,1]\\ \psi_T(X,0) = 0 & X \in [0,1]\\ \psi(0,T) = \psi(1,T) = \frac{\pi}{2} & T \in [0,\infty)\end{cases} \tag{23}$$

4.1. **Linear analysis for the dissipation-dominated case.** Following the procedure from [25], we analyze the Fréedericksz transition dynamics in the dissipation-dominated case. Also, for the present analysis, we make the one-constant approximation ($\alpha = \beta$). Disregarding the inertial term in (13), we consider the following simplified form of (15),

$$\tilde{\kappa}\psi_T = \tilde{\lambda}^2\psi_{XX} + \tilde{\varepsilon}\tilde{d}'(\psi)(u_X)^2 \tag{24}$$

$$\left(\tilde{d}(\psi)u_X\right)_X = 0 \tag{25}$$

for the initial data

$$\psi(X,0) = \psi_0(X), \quad \left|\psi_0(X) - \frac{\pi}{2}\right| \ll 1 \tag{26}$$

and boundary conditions

$$\psi(0,T) = \psi(1,T) = \frac{\pi}{2}, \quad u(0,T) = 0, \quad u(1,T) = 1. \tag{27}$$

By introducing $\theta = \psi - \pi/2$ we can linearize (24) around $\theta = 0$ to obtain

$$\tilde{\kappa}\theta_T = \tilde{\lambda}^2\theta_{XX} + 2\tilde{\varepsilon}\frac{\varepsilon_a}{\varepsilon_\perp}(u_X)^2\theta \tag{28}$$

$$u_{XX} = 0. \tag{29}$$

Notice that in this case (29) simply implies $u_X = 1$. Furthermore, we can introduce

$$\eta = \frac{\tilde{\lambda}^2}{\tilde{\kappa}}T \quad \text{and} \quad c = 2\frac{\tilde{\varepsilon}}{\tilde{\lambda}^2}\frac{\varepsilon_a}{\varepsilon_\perp} \tag{30}$$

as well as the transformation

$$\theta(X,\eta) = \Theta(X,\eta)\exp(c\eta) \tag{31}$$

in order to write (28) as

$$\Theta_\eta = \Theta_{XX}. \tag{32}$$

By standard techniques, the solution to (32) can be written in the form

$$\Theta(X,\eta) = \sum_{n=1}^{\infty} A_n \sin(n\pi X)\exp\left(-(n\pi)^2\eta\right) \tag{33}$$

which gives the solution

$$\theta(X,T) = \sum_{n=1}^{\infty} A_n \sin(n\pi X)\exp\left(-\frac{T}{\tau_n}\right), \tag{34}$$

with

$$\tau_n = \frac{\tilde{\kappa}}{2\frac{\varepsilon_a}{\varepsilon_\perp}\tilde{\varepsilon}_{\mathrm{c}}\left(n^2 - \frac{\tilde{\varepsilon}}{\tilde{\varepsilon}_{\mathrm{c}}}\right)}, \tag{35}$$

where we have introduced the critical non-dimensional electric field

$$\tilde{\varepsilon}_{\mathrm{c}} := \frac{1}{2}\frac{\varepsilon_\perp}{\varepsilon_a}\pi^2\tilde{\lambda}^2. \tag{36}$$

From (34) we see that all Fourier modes decay exponentially if $\tilde{\varepsilon} < \tilde{\varepsilon}_{\mathrm{c}}$. For $\tilde{\varepsilon} > \tilde{\varepsilon}_{\mathrm{c}}$ the initial state is not linearly stable and we get the onset of the Fréedericksz transition. For a near-critical electric field $\tilde{\varepsilon} > \tilde{\varepsilon}_{\mathrm{c}}$, it is then natural to define the switch-on time as [25]

$$\tau_{\mathrm{on}} =: -\tau_1 = \frac{\tilde{\kappa}}{2\frac{\varepsilon_a}{\varepsilon_\perp}\tilde{\varepsilon}_{\mathrm{c}}\left(\frac{\tilde{\varepsilon}}{\tilde{\varepsilon}_{\mathrm{c}}} - 1\right)}. \tag{37}$$

4.2. **Numerical experiments.** We wish to numerically study the evolution of the numerical solution compared to the stationary solution for different values of the parameters involved. To this end, we define the following: Let $\psi_{\mathrm{eq}}(X)$ be the stationary solution of (23). Given a solution $\psi(X,T)$, we define the normalized distance function

$$d_2(T) := \frac{\|\psi(\cdot,T) - \psi_{\mathrm{eq}}(\cdot)\|_{L^2}}{\|\psi(\cdot,0) - \psi_{\mathrm{eq}}(\cdot)\|_{L^2}}. \tag{38}$$

Numerical experiments were performed demonstrating how the dynamics of the Fréedericksz transition depends on the relationship between rotational inertia and the dissipation. We set $\delta = 0.01$ and the physical parameters $\beta/\alpha = 0.756$ and $\varepsilon_a/\varepsilon_\perp = 1.643$, consistent with the liquid crystal 5CB [25]. Moreover, we let $\tilde{\lambda} = 1$ and $\tilde{\varepsilon} = 100$, thereby ensuring that we are well above the critical electric field $\tilde{\varepsilon}_{\mathrm{c}} \approx 3$ for the onset of the Fréedericksz transition. The problem (23) was solved numerically using the finite-difference scheme (19)–(21) with $N = 100$. Figures 1, 2 and 3 show the numerical solution and distance (38) for $\tilde{\kappa} = 1$, 5 and 10, respectively. The results show that the presence of inertial forces causes standing waves to occur in the director field. For $\tilde{\kappa} = 1$ these are of a significant magnitude and cause the distance $d_2(T)$ to oscillate around zero. For stronger dissipation the standing waves are suppressed and the Fréedericksz transition is more monotone.

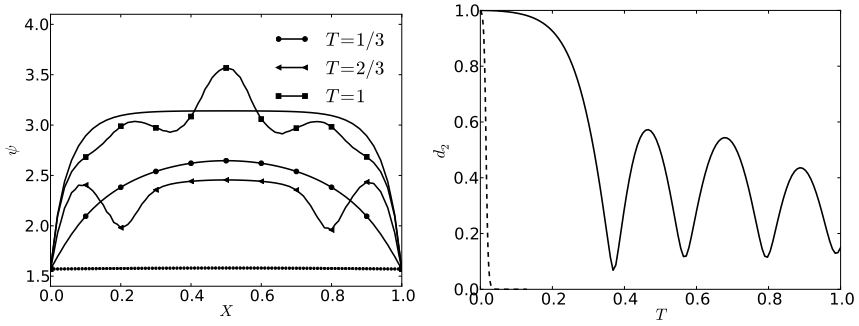

(A) ψ at different times (B) Distance from equilibrium (38)

FIGURE 1. The numerical solution of the homogeneous switch-on case (23) using $\tilde{\kappa} = 1$. Left: ψ at different times. The solid line is the stationary solution and the dotted line the initial data. Right: The evolution of the distance from equilibrium (38). The dashed line is the corresponding solution from the inertialess model (15).

In light of the standing waves seen in Figures 1, 2 and 3, we wish to determine the influence of these oscillations on the transition time from the initial state to the electrostatic equilibrium state. To that end, we in addition to (38) define the alternative distance function

$$e_2(T) := \frac{\|\psi(\cdot,T) - \psi(\cdot,0)\|_{L^2}}{\|\psi(\cdot,0) - \psi_{\mathrm{eq}}(\cdot)\|_{L^2}}. \tag{39}$$

While (38) is a normalized distance to the equilibrium, the function (39) gives the corresponding distance to the initial state. Using these we can now define the

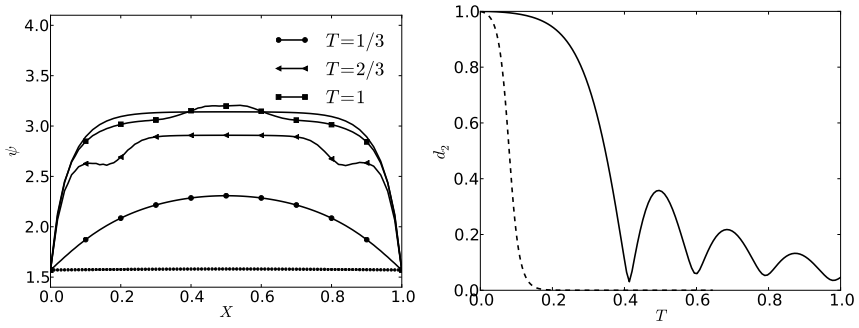

(A) ψ at different times (B) Distance from equilibrium (38)

FIGURE 2. The numerical solution of the homogeneous switch-on case (23) using $\tilde{\kappa} = 5$. Left: ψ at different times. The solid line is the stationary solution and the dotted line the initial data. Right: The evolution of the distance from equilibrium (38). The dashed line is the corresponding solution from the inertialess model (15).

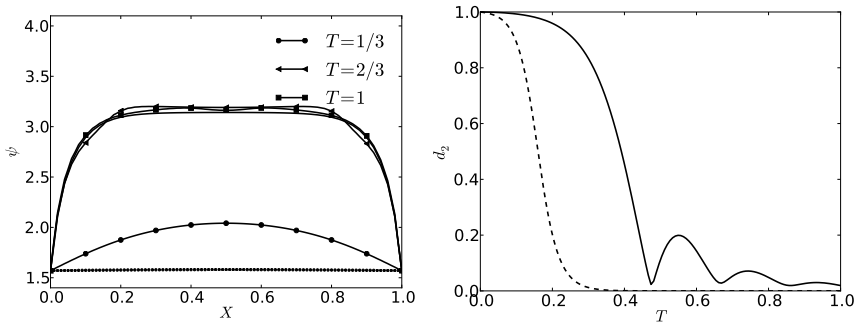

(A) ψ at different times (B) Distance from equilibrium (38)

FIGURE 3. The numerical solution of the homogeneous switch-on case (23) using $\tilde{\kappa} = 10$. Left: ψ at different times. The solid line is the stationary solution and the dotted line the initial data. Right: The evolution of the distance from equilibrium (38). The dashed line is the corresponding solution from the inertialess model (15).

switch-on time

$$T_* := \sup\{T : e_2(T) < \mathrm{e}^{-1}\} \tag{40}$$

and the *relaxation time*

$$T^* := \sup\{T : d_2(T) > \mathrm{e}^{-1}\}. \tag{41}$$

Figure 4 shows the switch-on and relaxation time using the definitions above. As before, the numerical solutions were obtained using $N = 100$ with $\tilde{\lambda} = 1$. We set the physical parameters to $\beta/\alpha = 0.756$ and $\varepsilon_a/\varepsilon_\perp = 1.643$. For large values of $\tilde{\kappa}$ the transition times are close to linear, a result that agrees with the characteristic time scale (37) from the linear analysis. However, when the inertial terms become

significant, the standing waves cause and increase in the relaxation time. This effect does not influence the switch-on time.

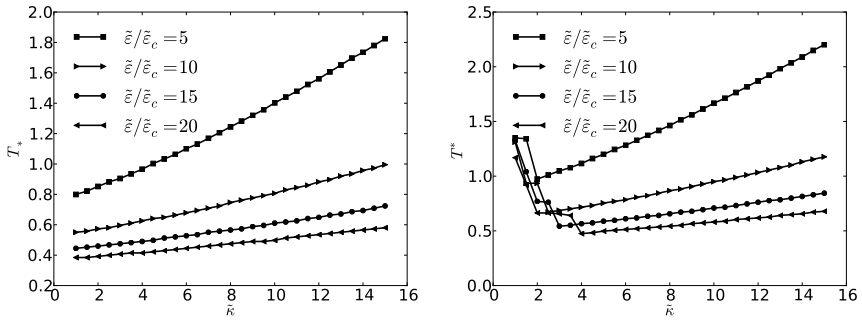

(A) Switch-on time (B) Relaxation time

FIGURE 4. Transition times for $\tilde{\lambda} = 1$ as a function of $\tilde{\kappa}$ for different values of the scaled non-dimensional electric field.

Figure 5 shows the switch-on and relaxation time as a function of the scaled non-dimensional electric field. Here, the linear analysis predicts an inverse relationship (37). Indeed, the results indicate that this is also the case for the full transition. However, also in this case the standing waves for low $\tilde{\kappa}$ increase the relaxation time, as shown in Figure 5b.

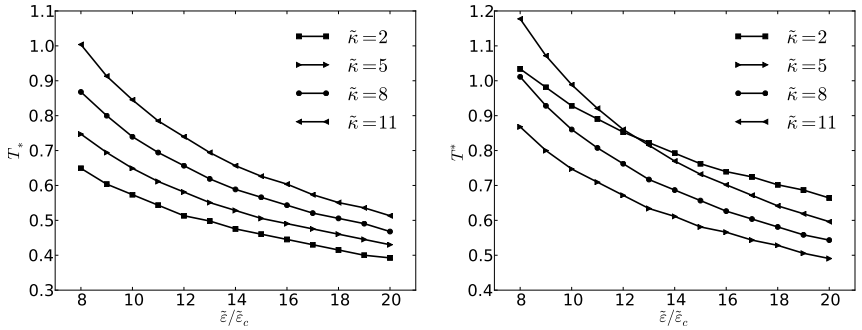

(A) Switch-on time (B) Relaxation time

FIGURE 5. Transition times for $\tilde{\lambda} = 1$ as a function of $\tilde{\varepsilon}/\tilde{\varepsilon}_c$ for different values of the non-dimensional dissipation constant.

Figure 7 shows the switch-on time (40) and the relaxation time (41) for the current model compared to the inertialess model (15) over a wide range of $\tilde{\kappa}$. As expected, the models seem to agree in the dissipation dominated limit $\tilde{\kappa} \to \infty$. However, a significant difference in transition times becomes apparent when $\tilde{\kappa}$ approaches ~ 10 from above. Values for the viscous constant κ are usually reported in the order of $10^{-1}\,\mathrm{Pa\,s}$ [25]. Quoted values for the rotational inertia varies from 10^{-11}–$10^{-16}\,\mathrm{kg\,m^{-1}}$ [7, 29]. Even with the highest reported values for the molecular inertia, $\tilde{\kappa} \sim 10$ still requires time scales in the nano-second range. This is outside

the physical domain of most current liquid crystal devices and experiments—the effect of inertia is here rightfully ignored.

We note that, under extreme conditions and within small time scales, inertial effects can become significant in the dynamics of the Fréedericksz transition. To illustrate this, we consider the Fréedericksz transition in the liquid crystal 5CB (with the physical parameters as before according to [25] and an estimated rotational inertia of $\sigma = 10^{-13}\,\mathrm{kg\,m^{-1}}$) under the influence of a strong electric field ($U_L = 5.00 \times 10^4\,\mathrm{V}$). As length scale and thickness of the liquid crystal sample we choose as before $L = 10^{-6}\,\mathrm{m}$, and as the time scale we let $\tau = 2 \times 10^{-11}\,\mathrm{s}$. This gives the non-dimensional parameters $\tilde{\kappa} = 15.5$, $\tilde{\lambda} = 1.8 \times 10^{-4}$, and $\tilde{\varepsilon} = 3.1 \times 10^2$. The plots in Figure 6 as well as the resulting switch-on time $T_* = 0.1040$ (0.0715 without inertia) and relaxation time $T^* = 0.1375$ (0.0865 without inertia) show the qualitative and quantitative effect of including inertia in this case.

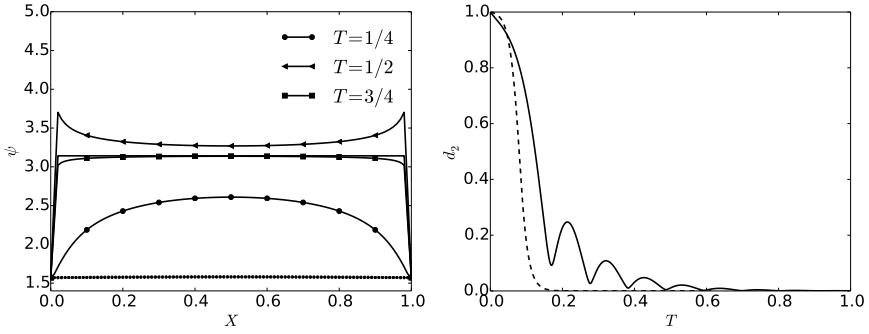

(A) ψ at different times (B) Distance from equilibrium (38)

FIGURE 6. The numerical solution of the homogeneous switch-on case (23) for physical values of the inertia and dissipation coefficient. Left: ψ at different times. The solid line is the stationary solution and the dotted line the initial data. Right: The evolution of the distance from equilibrium (38). The dashed line is the corresponding solution from the inertialess model (15).

Two other experiments where inertia becomes significant were suggested by Yun [29]. In the first one, the liquid crystal is subjected to a rapidly rotating magnetic field that is turned off abruptly. In the second one, the magnetic field is assumed to oscillate, leading to oscillations also in the director field with amplitude and phase lag depending on the inertia.

Finally we note that, because of the small time scales involved, the inclusion of inertia might also be warranted in, e.g., models for liquid crystal systems under high-frequency mechanical vibrations [27], liquid crystal acoustics [14] and studies of the light-induced Fréedericksz transition [17].

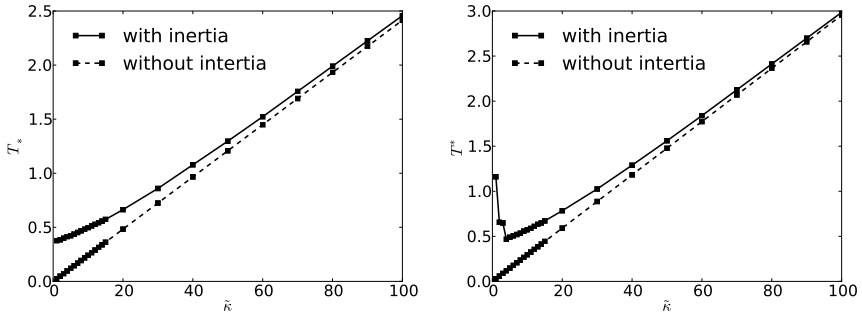

(A) Switch-on time (B) Relaxation time

FIGURE 7. Transition times for the inertialess model (15) compared to the current model for $\tilde{\lambda} = 1$ and $\tilde{\varepsilon}/\tilde{\varepsilon}_c = 20$.

5. The pi-cell

We now consider the transition from a stationary non-trivial initial state when applying an electric field. More precisely, we consider the initial-boundary problem (42)

$$\begin{cases} \psi_{TT} + \tilde{\kappa}\psi_T - \tilde{\lambda}^2\tilde{c}(\psi)\left(\tilde{c}(\psi)\psi_X\right)_X - \tilde{\varepsilon}\tilde{d}'(\psi)u_X^2 = 0, & (X,T) \in [0,1]\times[0,\infty) \\ u_X = \frac{1}{\tilde{d}(\psi)}\left(\int_{[0,1]}\frac{1}{\tilde{d}(\psi)}\mathrm{d}\xi\right)^{-1} & \\ \left(\tilde{c}(\psi)\psi_X\right)_X = 0, & X \in [0,1], T = 0 \\ \psi(0,T) = -\frac{\pi}{2} + \psi_{bc} & T \in [0,\infty) \\ \psi(1,T) = \frac{\pi}{2} - \psi_{bc} & T \in [0,\infty) \end{cases}$$

This experiment was studied by Mottram and Newton [23] in the stationary case using the one-constant approximation ($\alpha = \beta$) and by ignoring the inertial term. Note that in that case the equilibrium solution of (42) without electric field is a linear profile, while for the present nonlinear model it is nontrivial.

As before, we perform numerical experiments in order to study the dynamics of the transition occurring when applying an electric potential over the liquid crystal cell. For the initial data we follow Mottram and Newton [23] and use the equilibrium solution for the equation without electric field. In the nonlinear case $\alpha \neq \beta$ this solution is calculated numerically beforehand. For the boundary condition we define the parameter $\psi_{bc} = \pi/30$. Furthermore, we let $\tilde{\lambda} = 1$ and set the non-dimensional electric field to $\tilde{\varepsilon} = 100$. Figures 8, 9 and 10 show the numerical solution and the distance (38) for $\tilde{\kappa} = 1$, 5 and 10, respectively. The physical parameters were $\beta/\alpha = 0.756$ and $\varepsilon_a/\varepsilon_\perp = 1.643$, consistent with the liquid crystal 5CB [25]. The results all agree with the qualitative behavior that was observed for the homogeneous switch-on case. When dissipative forces are weak (compared to inertial forces) the initial part of the transition happens faster, but standing waves slow down the final relaxation towards equilibrium.

Similarly as in previous section, we now look at the transistion times (40) and (41) under variations of the electric field and rate of dissipation. Figure 11 shows the switch-on and relaxation time as a function of the non-dimensional dissipation $\tilde{\kappa}$. The numerical solutions were obtained using $N = 100$ with $\tilde{\lambda} = 1$ with physical

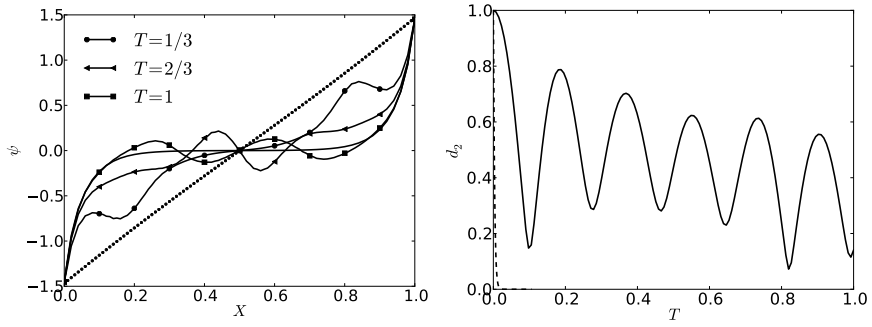

(A) ψ at different times (B) Distance from equilibrium (38)

FIGURE 8. The numerical solution of the Pi-cell intial value problem (42) using $\tilde{\kappa} = 1$. Left: ψ at different times. The solid line is the stationary solution and the dotted line the initial data. Right: The evolution of the distance from equilibrium (38). The dashed line is the corresponding solution from the inertialess model (15).

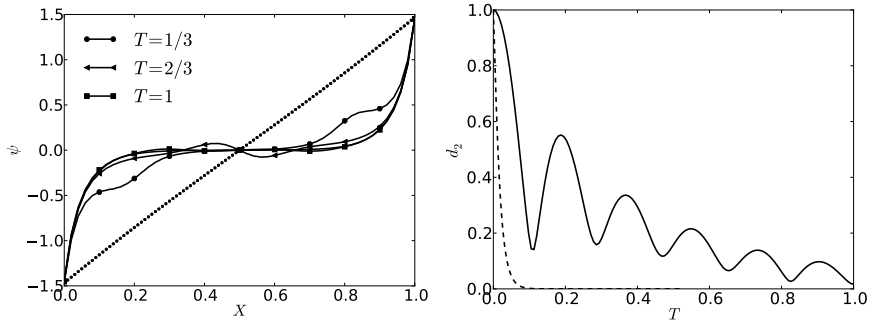

(A) ψ at different times (B) Distance from equilibrium (38)

FIGURE 9. The numerical solution of the Pi-cell initial value problem (42) using $\tilde{\kappa} = 5$. Left: ψ at different times. The solid line is the stationary solution and the dotted line the initial data. Right: The evolution of the distance from equilibrium (38). The dashed line is the corresponding solution from the inertialess model (15).

parameters to $\beta/\alpha = 0.756$ and $\varepsilon_a/\varepsilon_\perp = 1.643$. We note that also for the Pi-cell we have that the transition times are close to linear for large values of $\tilde{\kappa}$. Furthermore, when the $\tilde{\kappa}$ approaches 5 from above we observe an increase in the relaxation time due to the formation of standing waves.

Figure 12 shows the switch-on and relaxation time as a function of the scaled non-dimensional electric field. Also here, the results agree (for large $\tilde{\kappa}$) with the inverse relationship (37) predicted by the linear analysis. However, also in this case we observe an increase in the relaxation time, shown in Figure 12b.

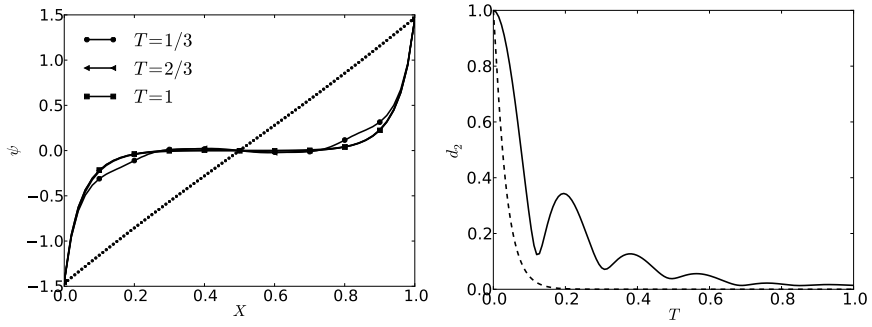

(A) ψ at different times (B) Distance from equilibrium (38)

FIGURE 10. The numerical solution of the Pi-cell intial value problem (42) using $\tilde{\kappa} = 10$. Left: ψ at different times. The solid line is the stationary solution and the dotted line the initial data. Right: The evolution of the distance from equilibrium (38). The dashed line is the corresponding solution from the inertialess model (15).

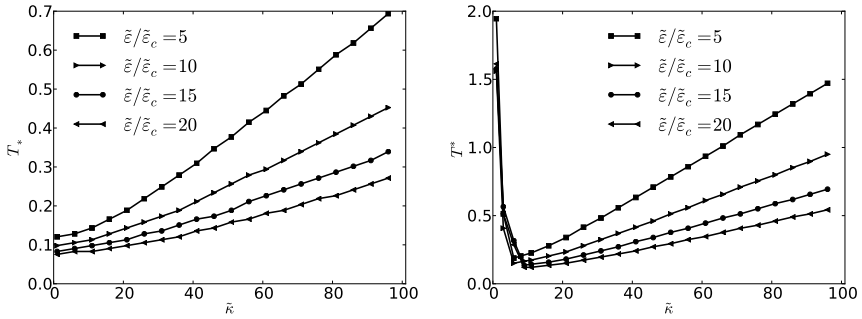

(A) Switch-on time (B) Relaxation time

FIGURE 11. Transition times for the Pi-cell intial value problem (42) using $\tilde{\lambda} = 1$, $\beta/\alpha = 0.756$ and $\varepsilon_a/\varepsilon_\perp = 1.643$.

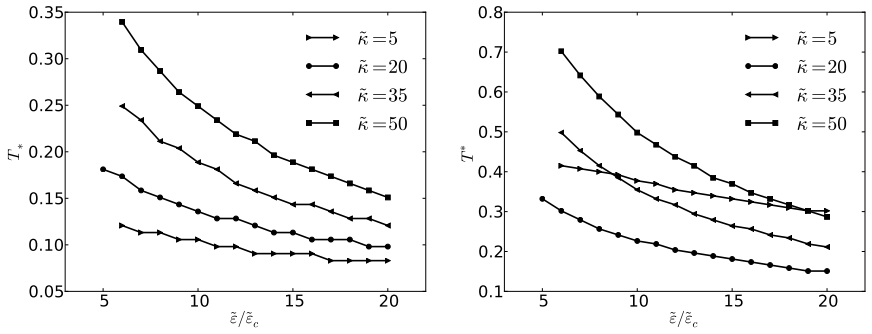

(A) Switch-on time (B) Relaxation time

FIGURE 12. Transition times for the Pi-cell intial value problem (42) using $\tilde{\lambda} = 1$, $\beta/\alpha = 0.756$ and $\varepsilon_a/\varepsilon_\perp = 1.643$.

6. Summary

We have derived a model for the dynamics of the director of a nematic liquid crystal under the influence of an electric field using an energy variational approach. Contrary to most of the literature, we have included both inertial forces and dissipation in our model. The model is coupled with the stationary Maxwell's equation for the electric field.

A semi-discrete numerical scheme has been proposed for solving the model. The method is an adaptation of a previously proposed scheme for a related variational wave equation modeling liquid crystals.

Numerical experiments have been performed demonstrating the influence of the relative strength between dissipative and inertial forces on two well-know cases from the literature. Both cases involve the reorientation of director field on a finite domain when applying an electric voltage. We observe that for moderate dissipation the transition times are proportional to the dissipation constant. However, when the scaling of the problem is such that the inertial term becomes dominant, this behavior breaks down as standing waves slow down or prevent the relaxation to electrostatic equilibrium.

Acknowledgements

The work of Peder Aursand and Johanna Ridder has been funded by the Research Council of Norway (project numbers 213638 and 214495, respectively).

The authors are grateful to Professor Nils Henrik Risebro and Professor Helge Holden for useful advice in the course of the preparation of this manuscript.

References

[1] G. Alì and J. K. Hunter. Orientation waves in a director field with rotational inertia. *Kinet. Relat. Models*, 2(1):1–37, 2009.

[2] G. Chen and Y. Zheng. Singularity and existence to a wave system of nematic liquid crystals. *J. Math. Anal. Appl.*, 398(1):170–188, 2013.

[3] P. G. de Gennes and J. Prost. *The Physics of Liquld Crystals*. Clarendon Press, Oxford, 1993.

[4] H. J. Deuling. Deformation of nematic liquid crystals in an electric field. *Molecular Crystals and Liquid Crystals*, 19(2):123–131, 1972.

[5] H. J. Deuling. Deformation pattern of twisted nematic liquid crystal layers in an electric field. *Mol. Cryst. Liq. Cryst.*, 27(1-2):81–93, 1974.

[6] B. J. Frisken and P. Palffy-Muhoray. Electric-field-induced twist and bend Fréedericksz transitions in nematic liquid crystals. *Phys. Rev. A*, 39(3):1513, 1989.

[7] X. Gang, S. Chang-Qing, and L. Lei. Perturbed solutions in nematic liquid crystals under time-dependent shear. *Phys. Rev. A*, 36(1):277–284, 1987.

[8] R. T. Glassey, J. K. Hunter, and Y. Zheng. Singularities of a variational wave equation. *J. Diff. Eq.*, 129(1):49–78, 1996.

[9] S. Gottlieb, C. W. Shu, and E. Tadmor. Strong stability-preserving high-order time discretization methods. *SIAM Rev.*, 43(1):89–112, 2001.

[10] H. Holden, K. H. Karlsen, and N. H. Risebro. A convergent finite-difference method for a nonlinear variational wave equation. *IMA J. Numer. Anal.*, 29(3):539–572, 2009.

[11] H. Holden and X. Raynaud. Global semigroup of conservative solutions of the nonlinear variational wave equation. *Arch. Rat. Mech. Anal.*, 201(3):871–964, 2011.

[12] J. K. Hunter and R. Saxton. Dynamics of director fields. *SIAM J. Appl. Math.*, 51(6):1498–1521, 1991.

[13] Y. Hyon, D. Y. Kwak, and C. Liu. Energetic variational approach in complex fluids: Maximum dissipation principle. *Disc. Cont. Dyn. Sys.*, 26:1291–1304, 2010.

[14] O. A. Kapustina. Liquid crystal acoustics: A modern view of the problem. *Crystallogr. Rep.*, 49(4):680–692, 2004.

[15] U. Koley, S. Mishra, N. H. Risebro, and F. Weber. Robust finite difference schemes for a nonlinear variational wave equation modeling liquid crystals. *ArXiv e-prints*, 2013.

[16] L. D. Landau and E. M. Lifshitz. *Statistical physics*, volume 5. Pergamon Press, Oxford, 1969.

[17] M. F. Ledney and O. S. Tarnavskyy. Influence of the anchoring energy on hysteresis at the Fréedericksz transition in confined light beams in a nematic cell. *Liq. Cryst.*, 39(12):1482–1490, 2012.

[18] E. K. Lenzi and G. Barbero. Relaxation of the nematic deformation when the distorting field is removed. *Phys. Rev. E*, 81:021703, 2010.

[19] F. M. Leslie. Theory of flow phenomena in liquid crystals. *Adv. Liq. Cryst.*, 4:1–81, 1979.

[20] V. B. Lisin and A. I. Potapov. Nonlinear interactions between acoustic and orientation waves in liquid crystals. *Radiophysics and Quantum Electronics*, 38(1–2):98–101, 1995.

[21] E. H. MacMillan. *A theory of anisotropic fluids*. PhD thesis, University of Minnesota, 1987.

[22] G. A. Maximov. Generalized variational principle for dissipative continuum mechanics. In *Mechanics of Generalized Continua*, volume 21 of *Advances in Mechanics and Mathematics*, pages 297–305. Springer New York, 2010.

[23] N. J. Mottram and C. J. P. Newton. *Handbook of Visual Display Technology: Liquid crystal theorey and modelling.* Springer-Verlag, Berlin, 2012.

[24] R. A. Saxton. Dynamic instability of the liquid crystal director. In W. B. Lindquist, editor, *Contemporary Mathematics*, volume 100 of *Current Progress in Hyperbolic Systems, Providence, RI, USA, 1989.*, pages 325–330, 1989.

[25] I. W. Stewart. *The static and dynamic continuum theory of liquid crystals: a mathematical introduction.* Taylor & Francis, London, 2004.

[26] C. Z. van Doorn. Dynamic behavior of twisted nematic liquidcrystal layers in switched fields. *J. Appl. Phys.*, 46:3738–3745, 1975.

[27] V. A. Vladimirov and M. Y. Zhukov. Vibrational Fréedericksz transition in liquid crystals. *Phys. Rev. E*, 76:031706, 2007.

[28] Q. A. Wang and R. Wang. Is it possible to formulate least action principle for dissipative systems? *ArXiv e-prints*, 2012.

[29] C. K. Yun. Inertial coefficient of liquid crystals: A proposal for its measurements. *Phys. Rev. A*, 45(2):119–120, 1973.

(Peder Aursand)
Department of Mathematical Sciences,
Norwegian University of Science and Technology,
NO–7491 Trondheim, Norway.
E-mail address: peder.aursand@math.ntnu.no

(Johanna Ridder)
Department of Mathematics,
University of Oslo,
P.O.Box NO-1053, Blindern, Oslo-0316, Norway.
E-mail address: johanrid@math.uio.no